

The WARPS survey - II: The Log(N)-Log(S) relation and the X-ray evolution of low luminosity clusters of Galaxies

L.R. Jones^{1,2,7,9}, C. Scharf^{2,8}, H. Ebeling^{3,9}, E. Perlman^{2,4,7,8}, G. Wegner⁵, M. Malkan⁶ and D. Horner^{2,8}

ABSTRACT

The strong negative evolution observed in previous X-ray selected surveys of clusters of galaxies is evidence in favour of hierarchical models of the growth of structure in the Universe. A large recent survey has, however, contradicted the low redshift results, finding no evidence for evolution at $z < 0.3$ (Ebeling et al. 1997a). Here we present the first results from an X-ray selected, flux and surface brightness limited deep survey for high redshift clusters and groups of galaxies based on ROSAT PSPC pointed data. The log(N)-log(S) relation of all clusters in this survey is consistent with that from most previous surveys but occupies a flux range not previously covered ($> 6 \times 10^{-14}$ erg cm⁻² s⁻¹ total flux in the 0.5-2 keV band). At high redshifts ($z > 0.3$) the cluster luminosities are in the range $4 \times 10^{43} h_{50}^{-2}$ erg s⁻¹ to $2 \times 10^{44} h_{50}^{-2}$ erg s⁻¹, the luminosities of poor clusters. The number of high redshift, low luminosity clusters is consistent with no evolution of the X-ray luminosity function between redshifts of $z \approx 0.4$ and $z=0$, and places a limit of a factor of < 1.7 (at 90% confidence) on the amplitude of any pure negative density evolution of clusters of these luminosities, in contrast with the factor of ≈ 3 (corresponding to number density evolution $\propto (1+z)^{-2.5}$)

¹School of Physics and Space Research, University of Birmingham, Birmingham B15 2TT, UK. Email: lrj@star.sr.bham.ac.uk

²Laboratory for High Energy Astrophysics, Code 660, NASA/GSFC, Greenbelt, MD 20771, USA.

³Institute for Astronomy, 2680 Woodlawn Dr, Honolulu, HI 96822, USA

⁴Space Telescope Science Institute, Baltimore, MD 21218, USA.

⁵Dept. of Physics & Astronomy, Dartmouth College, 6127 Wilder Lab., Hanover, NH 03755, USA.

⁶Dept. of Astronomy, UCLA, Los Angeles, CA 90024, USA

⁷Visiting Astronomer, Kitt Peak National Observatory, National Optical Astronomy Observatories, which is operated by the Association of Universities for Research in Astronomy, Inc. (AURA) under cooperative agreement with the National Science Foundation.

⁸Visiting Astronomer, Cerro Tololo Interamerican Observatory, National Optical Astronomy Observatories, which is operated by the Association of Universities for Research in Astronomy, Inc. (AURA) under cooperative agreement with the National Science Foundation.

⁹Visiting Astronomer, Canada-France-Hawaii Telescope, operated by the National Research Council of Canada, the Centre National de la Recherche Scientifique de France and the University of Hawaii.

found in the EMSS survey at similar redshifts but higher luminosities. Taken together, these results support hierarchical models in which there is mild negative evolution of the most luminous clusters at high redshift but little or no evolution of the less luminous but more common, optically poor clusters. Models involving preheating of the X-ray gas at an early epoch fit the observations, at least for $\Omega_0=1$.

Subject headings:

1. Introduction

Measuring the evolution of clusters of galaxies is a powerful test of hierarchical models of the gravitational growth of structure in the Universe. The most massive clusters are rare and in many models (e.g. the Cold Dark Matter model) the majority are predicted to have formed in the relatively recent past via the merger of less massive clusters. The rate of evolution of the properties of the cluster population, such as the X-ray luminosity and temperature functions, over a wide range of cluster masses, can help discriminate between different model parameters and between different thermal histories of the dominant X-ray gas.

X-ray surveys of clusters have the advantage in principle of being relatively unbiased, since they are unaffected by projection effects. Indeed, the detection of diffuse X-ray emission represents direct evidence of a deep gravitational potential within which the hot intra-cluster gas is trapped. Furthermore, the X-ray properties of the hot gas can be directly related to the gravitating mass, inferred to be dominated by a dark component. However, the observational evidence for X-ray evolution has not always been consistent in detail, even from purely X-ray selected and X-ray flux limited samples. One of the first determinations of the local X-ray luminosity function (XLF) using an X-ray selected sample was by Piccinotti et al. (1982), using non-imaging detectors. The first claims of a measurement of evolution in the cluster XLF were by Edge et al. (1990) and Gioia et al. (1990). Edge et al. compiled a list of 46 clusters and concluded that strong negative evolution was observed, with the number density of clusters of high luminosity ($L_X > 10^{45} h_{50}^{-2} \text{ erg s}^{-1}$) increasing by a factor of ~ 10 over the redshift range $z=0.18$ to $z=0$. From the 67 clusters at $z > 0.14$ imaged in the *Einstein* Extended Medium Sensitivity Survey (EMSS), Gioia et al. (1990) and Henry et al. (1992) found evidence (at 3σ significance) for a lower rate of evolution: for example the number density of high luminosity clusters ($L_X \approx 6 \times 10^{44} h_{50}^{-2} \text{ erg s}^{-1}$) was found to increase by a factor of ≈ 5 between median redshifts of $z=0.33$ and $z=0.17$. Castander et al. (1995) found that the number density of lower luminosity clusters ($L_X \gtrsim 1 \times 10^{43} h_{50}^{-2} \text{ erg s}^{-1}$) also showed evolution, with a factor of ≈ 2 increase from the redshift range $0.2 < z < 0.55$ to $z=0$ (although we find a different result in this paper; see section 5.5).

Recent results have altered this picture of strong evolution dramatically. The first of several large cluster samples being derived from the ROSAT All-Sky Survey (the “brightest cluster

sample” or BCS) contains ≈ 200 clusters and shows *no* evidence for evolution of the XLF at low redshifts, with a change in normalisation of the XLF of a factor of $\lesssim 1.6$ (at 68% confidence; Ebeling et al. 1997a fig. 5) for luminosities of $L_X > 4.5 \times 10^{44} h_{50}^{-2} \text{ erg s}^{-1}$ between median redshifts of $z=0.21$ and $z=0$ (Ebeling et al. 1997b). Ebeling et al. (1995, 1997a) show that this inconsistency with the results of Edge et al. (1990) is due to the small sample size and unfortunate sampling in redshift space (together with a volume miscalculation) in the Edge et al. sample, and that the rate of evolution at $z < 0.3$ measured from a much larger sample is considerably smaller than previously thought.

At higher redshifts, the results of the very recent survey of Collins et al. (1997) contradict those of Castander et al. (1995). Collins et al. find that the number of low luminosity clusters at $z > 0.3$ shows no evolution, even though the Collins et al. survey was not complete for the most extended X-ray sources. The EMSS sample of Henry et al. (1992) has been reanalysed by Nichol et al. (1997) who replaced *Einstein* IPC fluxes with ROSAT PSPC fluxes for 21 clusters and discarded 7 objects as unlikely to be clusters (although this aspect relied heavily on whether the objects were resolved in the ROSAT PSPC). Nichol et al. still found evidence for evolution of the XLF but at a lower rate than that measured by Henry et al. At even higher redshifts, Luppino & Gioia (1995) found no evidence in the EMSS for further evolution between $0.6 < z < 0.8$ and $z \approx 0.33$ for clusters of similar luminosity ($L_X \approx 6 \times 10^{44} h_{50}^{-2} \text{ erg s}^{-1}$), although their small sample size meant that a factor of ≈ 2 in number density evolution was allowed between $z \approx 0.33$ and $z \approx 0.7$. It is worth noting that, despite apparently contrary claims about the presence of strong evolution, the EMSS XLF agrees well with that Ebeling et al. 1997a where the two samples overlap in redshift. The evolution seen in the EMSS is limited to $z > 0.3$ and thus not in conflict with the low redshift results.

Thus, the recent X-ray results suggest that the evolution of the luminosity function of clusters is less rapid than previously thought, but that there is still evidence for evolution of X-ray luminous systems at high redshifts ($z \gtrsim 0.3$). In contrast, optical surveys for distant ($z > 0.3$) clusters have found the number density of rich clusters at high redshifts to be approximately the same as measured locally (Gunn et al. 1986, Couch et al. 1991, Postman et al. 1996). This difference may be due to the highly non-linear dependence of the X-ray luminosity on mass, so that a small change in mass (and richness) results in a large change in luminosity.

Current X-ray selected and X-ray flux limited samples contain few clusters at high redshifts, and even fewer high redshift, low X-ray luminosity clusters. Here we describe the first results from the WARPS (Wide Angle ROSAT Pointed Survey) cluster/group survey. This X-ray selected, X-ray flux limited survey was designed primarily to measure the high redshift ($z > 0.3$) cluster XLF at lower luminosities than the EMSS ($L_X \gtrsim 3 \times 10^{43} h_{50}^{-2} \text{ erg s}^{-1}$), but it also contains groups of galaxies, which have lower luminosities than clusters and are therefore detectable at lower redshifts of $z \approx 0.1$, and nearby individual galaxies which have been resolved. In this paper we concentrate on the evolution of clusters of galaxies of $L_X > 3 \times 10^{43} h_{50}^{-2} \text{ erg s}^{-1}$. We assume that groups and clusters of galaxies form a continuous population, referring to the population simply as ‘clusters’,

and do not further distinguish groups of galaxies from clusters. Future papers will investigate the detailed properties of all these systems. The survey design places particular emphasis on a high level of completeness in both X-ray source detection and cluster identification. Our application of the X-ray source detection technique (VTP or Voronoi Tessellation and Percolation), the source classification and the survey calibration are described in Scharf et al. (1997) (hereafter Paper I). Based on a larger sample for which optical identifications are currently being obtained, a future paper will describe the WARPS cluster XLF. Here we present the X-ray log(N)-log(S) relation (i.e. the number of clusters as a function of flux) for the current, statistically complete sample of confirmed clusters, both at all redshifts and at high redshifts alone, and use it to constrain the evolution of the cluster XLF.

In Section 2 we describe the sample selection. The optical observations are described in Section 3, and the the log(N)-log(S) relations are presented in Section 4. In Section 5 a comparison is made with the predictions of various models of the growth of structure in the Universe. An appendix gives details of the X-ray K-corrections used. Unless otherwise stated, we use $q_0=0.5$ and $H_0=50 h_{50} \text{ km s}^{-1} \text{ Mpc}^{-1}$.

2. The Sample

Our sample is based on ROSAT Position Sensitive Proportional Counter (PSPC) X-ray data from 86 pointings with exposures >8 ks (up to 48 ks) and galactic latitude $|b| > 20^\circ$. We set a limit of $3.5 \times 10^{-14} \text{ erg cm}^{-2} \text{ s}^{-1}$ in detected flux within the energy range of 0.5-2 keV. The observed redshift range of clusters is from $z=0.1$ to $z=0.67$ with a mean redshift ≈ 0.25 ; X-ray luminosities range from $1 \times 10^{42} h_{50}^{-2} \text{ erg s}^{-1}$ to $2 \times 10^{44} h_{50}^{-2} \text{ erg s}^{-1}$ (0.5-2 keV).

We minimize the Galactic contribution to the X-ray background by selecting a lower bound to the bandpass of 0.5 keV. Importantly, this also minimizes the size of the instrumental point spread function (PSF), while maintaining a high signal from gas at the temperatures found in clusters of galaxies. We use the part of each PSPC X-ray image within radii of 3 arcmin to 15 arcmin, avoiding the target of the pointing at low radii and the shadow of the window support structure which moved with the (deliberate) spacecraft wobble at large radii. The instrumental PSF also degrades rapidly at off-axis angles >15 arcmin. The original targets of the PSPC observations were nearly all Active Galactic Nuclei (AGN), stars or nearby galaxies. Five of the 86 observation targets were clusters or groups of galaxies, which could introduce a small bias, since clusters cluster amongst themselves. However, in none of these fields was a serendipitous cluster found at a redshift near that of the original target (within $\Delta z=0.1$), and below we show that the conclusions of the paper are not affected if these five fields are ignored. The non-cluster extragalactic targets could in principal introduce a small bias, if, for example, some fraction were AGN in a supercluster. An initial check shows that the fraction of fields with extragalactic targets containing serendipitous clusters above our flux limit ($40 \pm 9\%$) is not significantly different from the fraction with galactic targets ($33 \pm 9\%$). We note that here there are 5 fewer fields in total

(86 rather than 91) than described in Paper I. This is because very bright stars or large nearby galaxies were found to mask a large fraction of these fields. The total survey sky area is 16.2 deg².

Here we only summarize the source detection and classification procedure, since a full description is given in Paper I. Each PSPC field is corrected for non-uniform exposure and vignetting using energy dependent exposure maps. The source detection algorithm is Voronoi Tessellation and Percolation, described by Ebeling and Wiedenmann (1993) and in Paper I. The algorithm is very general, not preferentially detecting sources of any particular size or shape. An isophotal threshold in X-ray surface brightness a small factor (typically 1.4) above the background level is computed for each field. The individual sources are formed by grouping together neighbouring photons that lie above the surface brightness threshold. To help separate close sources which can be combined incorrectly into one source, the algorithm is rerun using 3-5 increasing threshold levels, and the final source catalogue compiled using the results from all thresholds. The 10th and 90th percentiles of the local thresholds for our final source list are 1.5 (for very extended, faint sources) and 3.0 (for deblended point sources), respectively.

Knowing the surface brightness threshold used for each source, the counts above the threshold, and the sky area in which they were detected, the total count rate extrapolated to infinite radius is calculated for each source assuming that the source profile is given by (a) the position-dependent PSF only, and (b) the PSF convolved with the best fit King profile. We assume that $\beta = \frac{2}{3}$, the average value found by Jones & Forman (1984), and measure the angular core radius (Ebeling et al. 1996, 1997b). A source is classified as extended if the ratio of the total fluxes calculated using the two assumptions exceeded a critical value determined from simulations (see Paper I).

A conversion from count rate to (absorbed) flux in the 0.5-2 keV band was performed using a constant factor of 1.15×10^{-11} erg cm⁻² s⁻¹ (ct s⁻¹)⁻¹. The maximum Galactic equivalent column density of neutral hydrogen (N_H) in the direction of our fields is 1.4×10^{21} cm⁻², and 90% of the fields have N_H in the range from 9×10^{19} cm⁻² to 7×10^{20} cm⁻². For this range of column density, and abundances of 0.25 times the cosmic abundance, even with Raymond & Smith (1977) spectrum temperatures of 1.4 keV to 14 keV the constant flux conversion factor is accurate to within 6%, and thus no correction for absorption variations has been made. The constant correction to unabsorbed fluxes (i.e. removing the effect of Galactic absorption) was made using a factor of 1.1, corresponding to the median N_H of 3.5×10^{20} cm⁻². This factor is almost independent of temperature and varies by $\pm 10\%$ within the above temperature and N_H ranges.

The correction from detected flux to total flux (i.e. extrapolated to infinite radius, but remaining in the 0.5-2 keV band) for extended sources which have been confirmed as clusters is typically a factor of 1.4 (but is computed for each source separately). A plot of total flux versus detected flux is shown in Figure 1 for all candidate clusters. A few point-like sources, for which the flux correction is small, are clearly visible close to the dashed line defining zero correction. These are cluster candidates which have been identified via our optical imaging program of point-like sources. The survey is complete to a flux limit in total flux of 6×10^{-14} erg cm⁻² s⁻¹ (0.5-2 keV),

higher than the flux limit of 3.5×10^{-14} erg cm $^{-2}$ s $^{-1}$ (0.5-2 keV) in detected flux (shown by the dotted lines). The measured core radii of resolved sources are typically in the range 0.3 arcmin to 0.6 arcmin. Simulations, shown in Figures 5 & 6 of Paper I show that in this range of core radii the total flux is recovered to within 10% accuracy for all signal to noise ratios and off-axis angles used, at least for the well-behaved King profiles used in the simulations. For a typical high redshift cluster in the survey at $z=0.5$ with a luminosity of $L_X \approx 1 \times 10^{44}$ h $_{50}^{-2}$ erg s $^{-1}$, a core radius of 0.40 arcmin corresponds to $r_c=170$ h $_{50}^{-1}$ kpc ($q_0=0.5$). Since this core radius is in reasonable agreement with those measured for nearby clusters, we are confident that the total count rates for most of our clusters, or at least those which are well described by a King profile, are accurate to within 10-20 per cent.

The sky area in which a source of a given total flux and intrinsic core radius could have been detected (including point sources) has been calculated via a combination of simulations and an analytical approach, as described in Paper I. The different exposure and background level of each PSPC field, and the position dependent PSF are all taken into account. The fraction of the total survey area available as a function of total flux and intrinsic core radius is given in Figure 8 of Paper I. In practice few sources of large angular size (core radius >0.7 arcmin) have been detected, although the survey was sensitive to them, and most of the extended sources, with core radii in the range 0.3 to 0.6 arcmin, could have been detected within $>90\%$ of the total survey area. In Section 5.4 below, we estimate how many large, very low surface brightness sources we expect in our survey, and find that the survey was sensitive to nearly all the sources predicted above the flux limit - i.e. the survey was nearly completely flux limited rather than surface brightness limited.

3. Optical observations

Here we describe the method used to categorize the optical counterparts and the action taken in the optical follow-up program. Because most high latitude X-ray sources at the fluxes considered here are AGN (e.g. Shanks et al. 1991), we select cluster and group candidates for spectroscopy based on the X-ray extent, sky survey plate measurements and CCD imaging.

Although clusters of core radii of 7 arcsec can be resolved on axis if the signal-to-noise ratio of the PSPC X-ray data is high, a more realistic limit, including off axis data, is ≈ 20 arcsec (see Figure 7 of Paper I), which corresponds to 140 h $_{50}^{-1}$ kpc at $z=0.5$. This resolution is adequate to resolve most clusters and groups with average core radii for their luminosity at the redshifts we expect to detect them (e.g. the mean core radius found by Jones & Forman 1984 for low redshift clusters was 250 h $_{50}^{-1}$ kpc). However, clusters have a wide range of morphologies (even within a small range of X-ray luminosity) and cooling flow clusters, unusually compact systems, or those which contain both extended emission and point sources could be classified erroneously as point-like (see Evrard & Henry 1991). Edge et al. (1992) measured substantial cooling flows ($>100 M_{\odot}$ yr $^{-1}$) in 23% (5 of 22) clusters with luminosity $<3 \times 10^{44}$ erg s $^{-1}$, indicating that cooling flows may be relatively common even in low luminosity systems. Cooling flows produce a peaked

X-ray surface brightness profile. For instance, Nichol et al. (1997) report that an HRI image of the luminous EMSS cooling flow cluster MS2137.3-2353 at a redshift of $z=0.313$ gives a core radius of 17 ± 8 arcsec, corresponding to $95 h_{50}^{-1}$ kpc. MS1512.4+3647, at a redshift of $z=0.373$, has an even smaller core radius of 7 ± 1.5 arcsec (Hamana et al. 1997). Sources with core radii this small may not be resolved in the PSPC (depending on off-axis angle), and therefore to maximise the completeness we include in the spectroscopic follow-up both extended sources regardless of their optical counterparts *and* point-like X-ray sources which have an excess of galaxies on R band CCD images. We do not include point-like X-ray sources which have only stellar optical counterparts (AGN and stars).

First, APM machine measurements of Palomar E and O and UKST R and B_j plates are obtained at the positions of all X-ray sources of flux $>3.5 \times 10^{-14}$ erg cm $^{-2}$ s $^{-1}$ (0.5-2 keV) at off-axis angles <15 arcmin. This gives typically 3-4 sources per field plus the target of the observation. The systematic PSPC pointing error, which is ~ 15 arcsec in size and varies in direction between observations (Briel et al. 1995), was removed by inspection of the optical maps at the positions of point X-ray sources, including the target of the observation where available. In nearly all fields the pointing error could be immediately determined to within ≈ 5 arcsec, since most of these X-ray sources have a single optical counterpart with a similar offset from the X-ray position as the target. The mean offset of these sources is taken as the X-ray pointing error. Possible optical counterparts with magnitudes near the plate limits are ignored in this procedure. The remaining random position errors for point X-ray sources are of mean (and 95%) size 4.7 ± 0.6 (9.7) arcsec. These error circle sizes were confirmed during the spectroscopic follow-up. A sample of 21 spectroscopically confirmed AGN has a mean (and 95%) position error of 4.8 ± 0.6 (9.3) arcsec. An error circle radius of 10-15 arcsec was adopted, depending on the signal-to-noise ratio of the detection.

For all sources, the X-ray contours are overlaid on digitized versions of the optical plate material in search of obvious optical counterparts. Depending on whether the X-ray source is extended or not, we then proceed as follows:

If, for extended X-ray sources, there is an excess of bright ($R < 19$ mag) galaxies within the X-ray contours, optical spectra are obtained of between 2 and 6 galaxies. If at least 2 galaxies (in the case of 2 or 3 spectra) or at least 3 galaxies (in the case of 4 or more spectra) have very similar redshifts, the source is identified as a cluster. CCD R band images of most of these clusters have been obtained. If the redshifts are not similar, or there is no excess of galaxies on the plate, imaging to $R=23$ mag (or to $R=24.5$ mag or in the I band in some cases) is obtained, objects selected for spectroscopy, and the process repeated. In general, the objects selected for spectroscopy in cluster candidates are not only the brightest galaxies but also those objects (including stellar objects) near peaks in the X-ray surface brightness. This process is important in determining the fraction of X-ray emission *not* from the intra-cluster medium, and also in cases where no excess of galaxies are found to $R \sim 24$ mag at the position of an extended X-ray source. In these latter cases we have so far found that in each case the X-ray source is not truly extended,

but a blend of several very close point-like sources, and the counterparts include AGN and stars.

For point X-ray sources, the APM magnitudes and source extent measurement (the ‘stellarness’ parameter; Irwin, Maddox & McMahon 1994) of the optical counterpart(s) are used to define the next action. If the error circle is blank, imaging to R=22 mag or fainter is obtained. If the error circle contains only faint APM objects, within 1 magnitude of the plate limit, then the APM source extent measurement is assumed to be unreliable and again R band imaging is obtained. In addition, if the X-ray extent parameter is in the range 1.1-1.2, just below the critical value of 1.2 above which a source is considered to be extended, CCD imaging is also obtained, regardless of the content of the error circle. If the CCD image contained an excess of galaxies in or close to the error circle, spectra were obtained of the galaxies as well as objects within the error circle. More usually, there was a single counterpart in the error circle. The FWHM of the counterpart was compared to stars on the same CCD image, and if it was at least 3σ greater than the mean stellar FWHM, the source was designated as a galaxy.

However, most ($\approx 70\%$) of the point X-ray sources contained a single counterpart within the error circle on the Palomar E or UKST R plates, and $\sim 70\%$ of these were bright enough to have an accurate APM ‘stellarness’ measurement (defined as R<19 mag for Palomar E plates and R<20 mag for UKST R plates). Where the object was detected on both blue and red plates, the mean stellarness parameter was used. A value of this parameter >1.8 defined an object as a galaxy. The units of this parameter are Gaussian standard deviations from the the mean stellar value of zero, so the value of 1.8 is conservative since a few stellar sources will be included but no galaxies will be excluded.

We initially obtained spectra of galaxy counterparts of point-like X-ray sources, whether or not an excess of galaxies was observed. The first ≈ 15 cases where there was no galaxy excess were found to be exclusively broad-lined AGN (with $\text{FWHM} > 1000 \text{ km s}^{-1}$) or low luminosity, normal galaxies. We have thus assumed that the X-ray emission from point-like X-ray sources does not arise in intra-cluster or intra-group gas unless an excess of galaxies is observed at the X-ray position, in which case spectroscopy is required to determine the origin of the X-ray emission.

A large number of telescopes is being used in this work. R band CCD imaging has been performed at the MDM 1.3m telescope, the Lick 1m Nickel telescope, the KPNO 0.9m telescope, the CTIO 0.9m telescope, the MDM 2.4m telescope and the WIYN 3.5m telescope. Low resolution spectroscopy has been performed at the KPNO 4m telescope, the CFH 3.6m telescope, the Lick 3m Shane telescope and the MDM 2.4m telescope. Multi-object spectroscopy was used on these telescopes whenever possible.

Finally, we note a possible cause of incompleteness due to the optical follow-up strategy. Bright, unrelated stars falling in error circles containing the real, fainter counterparts could mask the true counterpart. If the X-ray source is extended, we obtain CCD imaging in any case, and a faint cluster would be visible unless the star was brighter than R ~ 15 mag. Only relatively faint (R ~ 19 mag) stars are numerous enough at high latitudes (~ 0.1 per error circle; Jones et al. 1991)

to significantly contaminate the extended source sample, and stars this faint mask a negligible area of sky. The small number of point-like X-ray sources with galaxy counterparts which are cluster candidates (4% of all point-like X-ray sources) suggests that masking of point-like X-ray sources by bright stars will also not be a significant cause of incompleteness.

3.1. Source identification summary

The total number of X-ray sources above the limit of 3.5×10^{-14} erg cm $^{-2}$ s $^{-1}$ (0.5-2 keV) in detected flux in the 86 fields is 283, and 54 of these are labelled as extended. Ten of the point-like sources are also cluster candidates based on CCD imaging, giving a total of 64 candidates. One large extended source is faint and of ‘patchy’ appearance, with no excess of galaxies within the X-ray contours on CCD images. The small number of X-ray photons in each peak (<10) suggests that it is a false source, caused by a merger of noise peaks and faint point sources, and we have removed this source from the sample. One other source, which was originally identified as 3 separate components, each a significant detection but below the flux limit, has been manually re-inserted in the candidate list because an excess of galaxies at the position of at least one component suggested that the source may be a cluster with a large degree of sub-structure.

In several of the extended sources, inspection of the X-ray contours and spatial photon distribution clearly shows that they are 2 or 3 close point sources merged together, and so they have been treated as separate point sources. Spectroscopy in 2 of these cases has confirmed the counterparts as AGN. Four extended sources are identified with nearby individual galaxies which have been resolved with an X-ray extent similar to the optical extent, and one extended source is identified with a stellar cluster. We will concentrate on those sources above the flux limit in total flux, although there are several clusters in the survey below this limit.

In total, there are 46 candidate clusters and groups of galaxies above the total flux limit of 6×10^{-14} erg cm $^{-2}$ s $^{-1}$ (0.5-2 keV), of which five are coincident with previously catalogued clusters. We have CCD imaging of all these candidates; in 31 cases there is a clear excess of galaxies within the X-ray contours. We have spectroscopically confirmed, and measured redshifts for, 27 of these 31. At least 10 of the remaining 15 cluster candidate error circles contain a spectroscopically confirmed broad-lined AGN which contributes sufficient flux to put any remaining extended component below the survey flux limit. We suspect that most of the X-ray emission in some of the other 5 candidates will not originate in a hot intra-cluster medium; however, until further spectroscopy is performed, we label these objects as “possible” clusters. We will construct log(N)-log(S) relations both with and without the “possible” clusters.

In four of the confirmed clusters the X-ray contours indicate that a significant level of emission arises in point sources within the sky area of the cluster, usually from galaxies within the cluster itself. In these cases an estimate of the flux from the point sources has been made and the flux subtracted from the total. All but one of these clusters are of low luminosity and at low

redshifts $z < 0.3$, and thus will not affect the conclusions based on the high redshift clusters in our sample. The individual galaxy luminosities are naturally expected to be the highest fraction of the intra-cluster medium luminosity in the lowest luminosity clusters.

3.2. Estimated redshifts

To estimate whether the redshift is above $z=0.3$ for the minority of clusters for which we have no spectroscopic measurement, we use the crude approximation that if the brightest cluster galaxy (BCG) has $R > 18$ mag, then the cluster has $z > 0.3$. This is based on the Hubble diagram results of Sandage (1972) and Hoessel Gunn & Thuan (1980) and is consistent with the clusters for which we do have redshifts. For $17.5 < R_{BCG} < 18.5$ we consider the photometric redshift estimate to be uncertain (partly because of the intrinsic scatter in the Hubble diagram and partly because of the uncertainty in some of our magnitude estimates). We show below that our conclusions, based on the high-redshift counts of clusters, are not sensitive to the magnitude chosen to divide the $z > 0.3$ and $z < 0.3$ samples.

4. Results

The integral $\log(N)$ - $\log(S)$ relation for all 31 optically confirmed clusters in the WARPS sample is shown in Figure 2, together with the data from other X-ray selected cluster surveys. Shown on the abscissa is total flux in the 0.5-2 keV band (all fluxes quoted are for the 0.5-2 keV band unless explicitly stated otherwise), where “total flux” refers to the flux extrapolated to surface brightnesses below the detection limit. The WARPS points (shown as solid circles) overlap in flux with the faint end of the *Einstein* EMSS and occupy the gap between the EMSS and the deep ROSAT survey of Rosati et al. (1995). An extrapolation of the ROSAT BCS counts at bright fluxes (Ebeling et al. 1997b; shown as many small circles), which have a slope of -1.39, is shown by the dashed line. The WARPS counts lie on this line above a flux of $\approx 1.5 \times 10^{-13}$ erg cm⁻² s⁻¹, but fall below the extrapolation at fainter fluxes. The WARPS $\log(N)$ - $\log(S)$ was constructed using a sky area calculated separately for each cluster, taking into account its total flux and its angular core radius. The sky area as a function of these two parameters is shown in Figure 8 of Paper I. The number density of confirmed clusters at total fluxes $> 6 \times 10^{-14}$ erg cm⁻² s⁻¹ (0.5-2 keV) is 1.8 ± 0.34 deg⁻².

The integral $\log(N)$ - $\log(S)$ relations from the four different surveys shown in Figure 2 are in reasonable agreement. We investigate the consistency between the WARPS and the EMSS results below, but first we note that the general consistency is particularly impressive because each of the four surveys used independent data (from two different X-ray missions) and, importantly, independent source detection algorithms. We thus have some confidence in the completeness of the samples.

A maximum likelihood fit of a power law $N(> S) = KS^{-\alpha} \text{ deg}^{-2}$ to the WARPS counts (using the method of Murdoch et al. 1973, which effectively fits the differential counts) at total fluxes between 6×10^{-14} and $5 \times 10^{-13} \text{ erg cm}^{-2} \text{ s}^{-1}$ yields $\alpha = 0.93_{-0.34}^{+0.36}$ and $K = 8.8 \times 10^{-13}$ when S is measured in $\text{erg cm}^{-2} \text{ s}^{-1}$. A Kolmogorov-Smirnov test confirms that the data are not significantly different from this power law fit (55% probability that the two are different). An extrapolation of the BCS (0.5-2 keV) counts predicts 3.1 clusters deg^{-2} at the WARPS total flux limit, compared to the $1.8 \pm 0.34 \text{ deg}^{-2}$ observed, and is rejected at a probability of $< 10^{-2}$ (even if all the possible clusters are included), showing that there is a statistically significant turnover. Although, at the flux level probed by WARPS, this turnover is largely due to the increased cosmological stretching of the survey volume, it also reflects the shape and amplitude of the high redshift cluster XLF.

To measure the slope, we make the simplifying assumption that the area of sky surveyed is independent of the angular core radius of the clusters. For the majority of the clusters (65%) with core radii between 0.25 arcmin and 0.6 arcmin, this is accurate to within 7%. A better method would be to perform a joint fit to determine the slopes in both flux and core radius. However, the effect of varying the value of the assumed constant core radius between 0.35 arcmin and 0.55 arcmin is to vary the measured slope between 0.93 and 0.97, a small variation given the statistical errors caused by the small numbers of clusters in the sample.

The short dashed line just above the WARPS points in Figure 2 indicates the $\log(N)$ - $\log(S)$ relation obtained when all the “possible” clusters are included. The change when these objects are included is small; there is an increase at the faint limit equal in size to the error bar just visible on the faintest WARPS point. A small constant additive correction of 0.04 deg^{-2} has been added to the WARPS integral $\log(N)$ - $\log(S)$ points to correct for the bright clusters at fluxes $> 1 \times 10^{-12} \text{ erg cm}^{-2} \text{ s}^{-1}$ that did not appear in the survey because the area of sky sampled was too small. The value of 0.04 deg^{-2} corresponds to a flux of $1.4 \times 10^{-12} \text{ erg cm}^{-2} \text{ s}^{-1}$ in the BCS $\log(N)$ - $\log(S)$ relation.

The BCS data of Figure 2 are taken directly from Ebeling et al. (1997b). The EMSS data are also taken from Ebeling et al. (1997b), who derived the EMSS counts using the appropriate sky coverage and correction to total flux. We follow Henry et al. (1992) and assume a constant core radius of 250 kpc for the EMSS clusters. We have corrected the EMSS counts from the *Einstein* 0.3-3.5 keV band to the ROSAT 0.5-2 keV band using a constant factor of 1.7, appropriate for a Raymond and Smith (1977) thermal spectrum of temperature 4 keV and abundances of between 0.25 and 1 times cosmic abundance. We note that this approximation gives results accurate to $\lesssim 5\%$ when applied to the BCS $\log(N)$ - $\log(S)$ of Ebeling et al. (1997b) derived in the 0.3-3.5 keV band correctly, using an individual temperature for each cluster.

Although the integral $\log(N)$ - $\log(S)$ relation of Figure 2 gives a good overview, detailed comparisons can be misleading because the data points within each survey are not statistically independent. In order to comment on, for example, the completeness of the EMSS in the light of

the WARPS results, we turn to the differential $\log(N)$ - $\log(S)$ relation of Figure 3 in which the error bars and the data points within each survey are all statistically independent. Figure 3 contains the same data as Figure 2. The EMSS points lie below the WARPS points but they are not significantly different ($\chi^2=2.54$ for 2 degrees of freedom (dof), corresponding to 28% probability that they arise from the same distribution). The maximum WARPS cluster counts produced by including the “possible” clusters is shown by the short dashed line.

The number of WARPS clusters at redshifts $z>0.3$ and above the total flux completeness limit is 12 (there are an additional 3 clusters below this flux limit which we do not consider further). Of these 12, 10 have measured redshifts, and 2 have redshifts estimated to be above $z=0.3$ from the magnitude of the brightest galaxy. The differential $\log(N)$ - $\log(S)$ relation of the high redshift clusters is shown in Figure 4. There is good agreement between the WARPS counts and the EMSS counts. The maximum and minimum WARPS $\log(N)$ - $\log(S)$ relations are shown as dashed lines in Figure 4. The maximum number of $z>0.3$ WARPS clusters is 18, if the “possible” clusters are included and the brightest galaxy magnitude corresponding to $z=0.3$ is assumed to be $R_{BCG}=17.5$ mag instead of $R_{BCG}=18$ mag. The minimum number of $z>0.3$ clusters is 10, if R_{BCG} at $z=0.3$ is taken to be 18.5 mag and we remove the 2 fields where the observation target was a high redshift cluster and which contained other high redshift clusters (although at very different redshifts from the targets).

The high redshift $\log(N)$ - $\log(S)$ relation is more sensitive to evolution than the $\log(N)$ - $\log(S)$ relation of clusters at all redshifts, and it is from the high redshift data that we will draw our conclusions about the rate of evolution of low luminosity clusters. First, though, we describe the models which we use to predict the number of clusters.

5. Predicted counts and models of cluster evolution

In order to predict the expected number of clusters as a function of flux and redshift, we first integrate the zero redshift XLF assuming no evolution of the XLF with redshift, but including K-corrections and the effect of the co-moving volume element for the assumed value of q_0 . We use the BCS zero redshift XLF of Ebeling et al. (1997a). The details of the K-correction, which is in general a 10%-20% effect, are given in an Appendix. We then investigate the effect of pure density evolution on the predicted $\log(N)$ - $\log(S)$ relation, and lastly compare the predictions of the more physically motivated evolution models of Mathiesen & Evrard (1997) with the data. All the models assume that all the X-ray flux within a given energy band from each cluster has been detected and that all the observational detection limitations have been removed. This is not quite true. The detected fluxes have been converted to total fluxes and corrections have been made (via the sky area surveyed) for the slightly lower detection probability of *detected* sources of large angular size compared with those of small size (for a given total flux). Sources will be missing from the survey if they are of such a large angular size that all their flux falls below our surface brightness threshold, even though the total flux is above the survey limit. This incompleteness,

including the effect of cosmological surface brightness dimming, is estimated in Section 5.4 and found to be small.

5.1. Clusters at all redshifts

The two smooth curves in Figure 2 show the predicted $\log(N)$ - $\log(S)$ relation for all clusters in the survey assuming no evolution of the XLF with redshift; the integration of the Ebeling et al. (1997a) 0.5-2 keV XLF was performed over the redshift range $0 < z < 2$ and the luminosity range $1 \times 10^{42} \text{ erg s}^{-1} < L_X < 1 \times 10^{47} \text{ erg s}^{-1}$, encompassing all detected cluster luminosities. At the flux limit of the WARPS survey there is little difference between the predictions for $q_o=0.5$ (lower curve) and $q_o=0$ (upper curve). Both curves fit the WARPS data and the Rosati et al. (1995) data well. For $q_o=0$ our use of the BCS XLF is not strictly valid, since the BCS XLF was derived assuming $q_o=0.5$. However, since the median BCS cluster redshift is $z \approx 0.1$, the effects of the assumed value of q_o on the value of the BCS XLF will be small.

In Figure 3 we quantify the similarity between a $q_o=0.5$ no-evolution model (shown as a solid line) and the observed differential $\log(N)$ - $\log(S)$ relations. The WARPS data are consistent with a no-evolution model, both including and excluding the “possible” clusters. The EMSS data lie slightly below the no-evolution model. Assuming only Poisson errors, the χ^2 for EMSS clusters at fluxes $> 10^{-11} \text{ erg cm}^{-2} \text{ s}^{-1}$ is 19.2 (for 8 dof), corresponding to 1% probability that the data are consistent with the no-evolution model. However, a systematic increase in flux by a factor of 1.25 in the EMSS data would make them consistent with the model (at 44% probability). A systematic error of that size is very possible, given the mean EMSS conversion factor from detected to total flux of 2.5 and the assumed constant core radius of 250 kpc (in contrast to WARPS where the core radius is estimated for each cluster independently, and the mean conversion factor from detected to total flux is 1.4). There is an additional small uncertainty in the conversion from the EMSS 0.3-3.5 keV band to the 0.5-2 keV band. Ebeling et al. (1997b) show that the difference in the EMSS counts introduced by assuming a constant core radius of 300 kpc instead of 250 kpc is a factor which varies with flux between values of ≈ 1.05 and 1.2, almost sufficient to account for the observed difference. We investigate in detail possible systematic differences between flux measurement methods in Appendix A, using ROSAT PSPC data of EMSS clusters, and find that the EMSS fluxes may be too small by a factor of ≈ 1.2 -1.3. Thus we conclude that the WARPS and EMSS all-redshift cluster $\log(N)$ - $\log(S)$ relations are in good agreement, especially if this correction is applied, and that they show no evidence for evolution of the XLF.

This is not inconsistent with the result of Henry et al. (1992), who found evidence for evolution at high redshifts in the EMSS data, since here we are not including any redshift information and the $\log(N)$ - $\log(S)$ relation blurs the differences between low and high redshifts. In the next section we examine the high redshift $\log(N)$ - $\log(S)$ relation separately in order to clarify the situation.

5.2. Clusters at high redshifts

In Figure 4 we show the predicted differential $\log(N)$ - $\log(S)$ relation for clusters at $z > 0.3$ assuming the same zero redshift XLF and integration limits as above (taking into account the lower limit imposed on luminosities by the $z > 0.3$ redshift limit, which is $2.6 \times 10^{43} \text{ erg s}^{-1}$ at the WARPS flux limit). The solid line is for $q_0 = 0.5$ and no-evolution; this is a good match to the WARPS data (which are dominated by the faintest bin). This is true for the range of $\log(N)$ - $\log(S)$ relations both including and excluding the possible clusters, as shown by the dashed lines. The EMSS data, however, fall systematically below the no-evolution prediction. Assuming Poisson statistics alone, the EMSS data are inconsistent with the no-evolution prediction ($\chi^2 = 20$ for 4 dof or $< 0.1\%$ probability) but a systematic flux increase by a factor of 1.25 in the EMSS data would remove the inconsistency ($\chi^2 = 3.0$ or 56% probability).

In order to quantify the level of evolution allowed by the data, we have predicted $\log(N)$ - $\log(S)$ relations assuming pure density evolution of the XLF $\phi(z)$ of the form

$$\phi(z) = \phi(0)(1+z)^{\alpha_D}$$

which is applied equally to all luminosities. This simple parameterisation provides a convenient description of the data for comparison with e.g. detailed hydrodynamic or N-body models of cluster evolution. The dashed lines in Figure 4 were calculated using $\alpha_D = -2$ and $\alpha_D = -3$. The $\alpha_D = -2$ parameterisation is consistent with the EMSS data, but $\alpha_D \leq -3$ is inconsistent with the WARPS data (at $< 1\%$ probability), and $\alpha_D = -2$ is only marginally inconsistent with the WARPS data (2% probability).

Although the $z > 0.3$ $\log(N)$ - $\log(S)$ relation of Figure 4 does not show evidence of inconsistency with the $q_0 = 0.5$ no-evolution prediction (given a possible EMSS systematic error), there is a trend in which the lowest (WARPS) flux point lies just above the prediction whereas the brightest (EMSS) flux points lie below the prediction, even if their flux is increased systematically by a factor of 1.25. We will thus check for differences between the WARPS and EMSS samples. One difference is the redshift distribution at $z > 0.3$. However, because the WARPS sample has a fainter limiting flux than the EMSS sample, it will have a higher mean redshift, and thus should show more evolution, not less, assuming any evolution is a monotonic function of redshift.

The more important difference between the WARPS and EMSS high redshift clusters is the range of X-ray luminosities covered by the two samples. The luminosities of the high redshift WARPS clusters lie in the range from $4 \times 10^{43} h_{50}^{-2} \text{ erg s}^{-1}$ to $2 \times 10^{44} h_{50}^{-2} \text{ erg s}^{-1}$ (0.5-2 keV, $q_0 = 0.5$), whereas the EMSS clusters lie in the range from $1 \times 10^{44} h_{50}^{-2} \text{ erg s}^{-1}$ to $1.5 \times 10^{45} h_{50}^{-2} \text{ erg s}^{-1}$ (0.5-2 keV, $q_0 = 0.5$). We will investigate whether the evolution rate is luminosity-dependent.

5.3. Different evolution at low and high luminosities

In Figures 5 and 6 we show the $\log(N)$ - $\log(S)$ relation for a restricted subset of clusters; high redshift ($z>0.3$), low luminosity clusters (Figure 5) and high redshift ($z>0.3$), high luminosity clusters (Figure 6). In both Figures the no-evolution prediction is shown by a solid line. The low luminosity clusters of Figure 5 include all the WARPS clusters at $z>0.3$ and 10 EMSS clusters with $L_X < 3 \times 10^{44} h_{50}^{-2} \text{ erg s}^{-1}$ (0.5-2 keV, $q_0=0.5$) where a conversion factor of 1.7 between the Einstein 0.3-3.5 keV and ROSAT 0.5-2 keV bands has been used (see Section 4). The EMSS and WARPS counts are in good agreement. Although there are large errors on both datasets, they are both consistent with the no-evolution prediction ($\chi^2=2.34$ for 2 dof, corresponding to 31% probability for the WARPS points, and $\chi^2=2.25$ for 3 dof, corresponding to 52% probability for the EMSS points, which have an even higher probability if their flux is increased by a factor of 1.25). As before, the prediction is based on the BCS zero redshift XLF which was integrated over $0.3 < z < 2$ and $10^{42} < L_X < 3 \times 10^{44} \text{ erg s}^{-1}$.

In contrast, the high luminosity clusters shown in Figure 6 fall a factor ≈ 2.5 -3 below the no-evolution prediction, which was obtained by integrating the zero redshift BCS XLF over $0.3 < z < 2$ and $3 \times 10^{44} < L_X < 10^{47} \text{ erg s}^{-1}$. There are no WARPS clusters with luminosities this high, so this Figure contains only data from the EMSS, for which $\chi^2=28.2$ (for 4 dof), corresponding to a probability of $< 10^{-4}$ that the data and the no-evolution prediction are consistent (assuming the error due to the small number of EMSS clusters dominates the error in the prediction). The probability is still only 1% ($\chi^2=13.1$) if a systematic flux increase of 1.25 is applied to the EMSS data. The negative evolution EMSS result of Henry et al. (1992), and the comparison of the EMSS and BCS luminosity functions of Ebeling et al. (1997a), is confirmed.

We parameterise evolution using the pure density evolution index α_D as before. The long dashed lines in Figures 5 and 6 show the predictions for various values of α_D , both positive and negative. The number of WARPS clusters observed at $z>0.3$, with total flux $> 6 \times 10^{-14} \text{ erg cm}^{-2} \text{ s}^{-1}$ (0.5-2 keV) and of low luminosity $L_X < 3 \times 10^{44} h_{50}^{-2} \text{ erg s}^{-1}$ is $0.73 \pm 0.34 \text{ deg}^{-2}$ (at 90% confidence), compared to the no-evolution prediction of 0.63 deg^{-2} and corresponding to $-1.2 < \alpha_D < +1.8$ (at 90% confidence). At the same redshift limit and the higher EMSS flux limit of $1.3 \times 10^{-13} \text{ erg cm}^{-2} \text{ s}^{-1}$ (0.5-2 keV), the number of high luminosity EMSS clusters ($L_X > 3 \times 10^{44} h_{50}^{-2} \text{ erg s}^{-1}$) observed is $0.053 \pm 0.021 \text{ deg}^{-2}$ (at 90% confidence), compared to the no-evolution prediction of 0.16 deg^{-2} and corresponding to $-3.5 < \alpha_D < -1.5$ (at 90% confidence), a significantly different range of α_D . If the EMSS flux limit is actually a factor of 1.25 higher, the no-evolution prediction becomes 0.13 deg^{-2} , corresponding to $-3 < \alpha_D < -1.3$.

The short dashed lines in Figure 5 show the possible range of the WARPS counts given the uncertainties due to the as yet unidentified cluster candidates, the clusters with estimated redshifts, and also include the effect of removing the two fields which had high redshift cluster targets. The effects of all these uncertainties is of similar size as the statistical error. The lowest possible WARPS counts are still consistent with no-evolution but inconsistent with $\alpha_D=-3$. The

highest possible WARPS counts may be more consistent with weak positive evolution than no evolution, but we cannot distinguish between these possibilities at this stage. We are in the process of expanding the sample size in order to investigate this possibility.

So far, we have only considered density evolution. An alternative is pure luminosity evolution in which the XLF scales only in luminosity with redshift, such that $L^*(z) = L^*(0)(1+z)^{\alpha_L}$ where L^* is the characteristic luminosity of the Schechter function XLF. Because the XLF is steepest at high luminosities, a single value of $\alpha_L \approx -1$ fits both the low luminosity and high luminosity high redshift $\log(N)$ - $\log(S)$ relations of Figs 5 & 6. Although this parameterisation is attractive because of its simplicity (it is independent of luminosity), pure luminosity evolution is not consistent with the high redshift luminosity function of Henry et al. (1992) when compared by Henry et al. with their lower redshift luminosity functions or when compared with the more accurately measured low redshift BCS luminosity function by Ebeling et al. (1997a).

5.4. Surface brightness dimming

The models described above assume that all the clusters above a given flux limit are detected and that the detected flux is corrected to a total flux. They omit surface brightness dimming effects which in principle could cause a cluster of large angular size to be missed completely from the survey. In this Section we estimate that the number of clusters missed because they fall completely below the surface brightness limit is a small fraction of the total.

We adopt a simple empirical approach. In order to predict the cluster angular core radius-flux distribution and compare it with the survey sensitivity, we need to assume a core radius-luminosity relation. Based on the virial theorem and simple scaling arguments (eg Kitayama & Suto 1996) we adopt

$$r_c = \frac{250}{h_{50}} \left(\frac{L_{44}}{5} \right)^{0.2} \quad kpc$$

where we have normalised the core radius r_c to be $250 h_{50}^{-1}$ kpc for a cluster of luminosity $L_{44} = 5$ in units of 10^{44} erg s^{-1} . We make the simplifying assumption that $\beta = \frac{2}{3}$ for all clusters. This relation is in reasonable agreement with the measurements of nearby clusters of Jones & Forman (1984) and Kriss et al. (1983). The mean Jones & Forman values of r_c for clusters with centrally dominant galaxies ('XD' clusters) agree with the above relation to within 25% for cluster luminosities of 10^{43} erg s^{-1} to 10^{45} erg s^{-1} and for β fixed at 0.6. For groups with luminosities $< 10^{43}$ erg s^{-1} the above relation is not such a good description, although the general trend is correct, and there is a large scatter in the observed core radii of local groups (eg Mulchaey et al. 1996).

Given the above relation, we integrate the BCS XLF of Ebeling et al. (1997a) over $0 < z < 2$ and $10^{42} < L_X < 10^{47}$ erg s^{-1} as described in Section 5 to obtain the predicted flux-angular core

radius distribution. The clusters are predicted to occupy a region of the flux-angular core radius plane to which WARPS has good sensitivity, as measured by the simulations described in Paper I. At the lowest fluxes (6×10^{-14} to 8×10^{-14} erg cm $^{-2}$ s $^{-1}$) and large core radii (>0.6 arcmin) the detection probability is $<80\%$. The fraction of clusters predicted within this flux range with core radii >0.6 arcmin is only 3% of the total number of clusters in the flux range. Virtually no clusters ($<1\%$) are predicted at core radii >0.8 arcmin within this flux range. This corresponds to a luminosity of 8×10^{43} h $_{50}^{-2}$ erg s $^{-1}$ and a core radius of 340 h $_{50}^{-1}$ kpc at a redshift of $z=0.5$ (for $q_0=0.5$). We would only be able to detect such objects in 40% of the survey area. At further extremes a cluster of core radius 1.2 arcmin (or 510 h $_{50}^{-1}$ kpc at $z=0.5$) at the flux limit would only be detectable in 10% of the survey area. Jones & Forman (1984) found that 4 out of 30 (13%) Abell clusters at $z < 0.06$ and $L_X < 10^{44}$ erg s $^{-1}$ had core radii >350 kpc, for $\beta=0.6$, and all of these were ‘nXD’ systems without centrally dominant galaxies. Only 2 out of 30 (7%) had core radii >500 kpc.

In general, clusters are predicted to mostly populate regions of the flux-angular core radius plane where the detection probability is high, at least in the WARPS survey. Of course, scatter in the $r_c - L_X$ relation and the inclusion of the less common clusters without centrally dominant galaxies will result in some clusters being lost from the survey, but we expect that the number lost in any flux range will be $\lesssim 10\%$ of the total, particularly at $z > 0.3$ where the cluster luminosities are always $>10^{43}$ erg s $^{-1}$, a luminosity range where the sizes have been well sampled, at least in the local Universe.

5.5. Comparison of the WARPS and RIXOS number count results

The RIXOS cluster survey of Castander et al. (1995) found strong evidence for negative evolution at redshifts $z > 0.3$ from a ROSAT survey to a similar flux limit and covering a similar area of sky as that used here. Since the conclusions of Castander et al. are quite different to ours, we investigate here possible reasons for the discrepancy.

Firstly we compare directly the surface density of $z > 0.3$ clusters, not including the instrumental effect of varying sensitivity across the PSPC field of view, as these are approximately the same for both surveys. RIXOS has 5 clusters at $z > 0.3$ from 14.9 deg 2 or 0.33 ± 0.15 deg $^{-2}$ above a detected flux of 3.0×10^{-14} erg cm $^{-2}$ s $^{-1}$ (0.5-2 keV). This flux limit is close to, but slightly less than, our limit of 3.5×10^{-14} in detected flux, and so if anything the RIXOS survey should measure a higher surface density of clusters. However, we find 14 $z > 0.3$ clusters from 16.2 deg 2 or 0.86 ± 0.22 deg $^{-2}$, 2.5 times the RIXOS density and significantly different at the 95% level.

In this paper we have taken the approach of correcting the measured source fluxes to obtain an estimate of the total flux from each cluster. Castander et al. take a different approach by assuming all clusters have the same core radius, modeling the detection of the clusters and including the detection efficiency in the $n(z)$ predictions obtained by integrating different

evolutionary XLFs. Although detailed comparisons between the two approaches are difficult to make, a comparison of the number of clusters detected relative to the prediction of the no evolution model in each case should take into account the differences. In the RIXOS survey, at $z > 0.3$ the number detected (5) is 0.28 times the number predicted (18) from Figure 1 of Castander et al. In WARPS the number detected (in the range of total flux where WARPS is complete at $z > 0.3$, i.e. 6×10^{-14} erg cm $^{-2}$ s $^{-1}$ - 2×10^{-13} erg cm $^{-2}$ s $^{-1}$) is at least 12, or 0.89 times the number predicted from the no-evolution model (for $q_0 = 0.5$ as used by Castander et al.). This is 3.2 times the number of clusters observed in the RIXOS survey (in each case relative to the no-evolution model), and this difference leads to the different conclusions in this paper and those of Castander et al.

One might think that the difference could be due to differences in the optical follow-up strategies. Castander et al. spectroscopically identified nearly all (95%) of the detected X-ray sources. Source classification here is based partly on X-ray extent and partly on optical imaging, so any difference due to the follow-up strategies would result in fewer clusters detections in WARPS, not more.

Another, more compelling, hypothesis is that the discrepancy between the WARPS and RIXOS results is due to fundamental differences in the X-ray source detection algorithms used in the two surveys. The RIXOS source detections were based partly on an algorithm optimised for point sources. As shown in Paper I, a point-source based algorithm will severely underestimate the flux from extended sources in the PSPC data. A systematic flux underestimate of 30% (less than the typical correction we apply for undetected flux below the surface brightness threshold) will also reduce the number of clusters by $\approx 30\%$ at the WARPS flux limit, partly explaining the discrepancy. If this is the case, RIXOS completeness might at first sight be expected to increase with redshift, since clusters of the same linear size will have a smaller angular size at higher redshift, and suffer less flux loss. However, at higher redshift, the constant survey flux limit means that clusters of higher luminosity and thus larger linear size will be observed, and the net result is that the mean angular size increases only slightly over the flux range where most clusters are detected ($\sim 6\text{-}20 \times 10^{-14}$ erg cm $^{-2}$ s $^{-1}$; see fig 8 of Paper I). Thus the RIXOS incompleteness should not be a strong function of redshift, at least at $z > 0.2$. Of course the use of a point source detection algorithm does not only entail the risk of systematically underestimating the fluxes of extended sources; the latter may be missed altogether even at intermediate redshifts.

6. Discussion

We have measured a luminosity-dependent rate of evolution for clusters of galaxies over the redshift range $z \approx 0.3\text{-}0.4$ to $z = 0$. Our result that the cluster X-ray luminosity function does not evolve at low luminosities (or at least evolves less negatively than at high luminosities) supports the hierarchical model of the growth of structure, in which less massive clusters require less time to form. The predictions of CDM using the Press-Schechter (1974) formalism as plotted in e.g.

Efstathiou & Rees (1988) and Peacock (1991) are that the number density of objects with the mass of X-ray luminous clusters evolves strongly over the range $z=0$ to $z=1$, whereas less massive objects are predicted to have less evolution. Observationally, our result is in agreement with the recent survey of Collins et al. (1997) but disagrees with Castander et al. (1995). There was also tentative evidence in the EMSS luminosity functions of Henry et al. (1992) and the comparison of the EMSS and BCS luminosity functions in Ebeling et al. (1997a) for different levels of evolution at different luminosities.

We have compared this initial dataset with a luminosity-dependent density evolution parameterisation. Realistically, a combination of both luminosity and density evolution is expected. The evolution of the hot gas density and hot gas mass will largely determine the luminosity evolution, while the number of clusters of a given mass in a hierarchical model depends on the rate of formation (from the merging of smaller clusters) and the rate of destruction (by merging into larger clusters). The combination of these effects determines the overall evolution of the XLF, which is thus dependent on the energetics of galaxy evolution (including the level of heat input into and cooling of the ICM) and on the cosmology and the primordial fluctuation spectrum.

6.1. Cosmological models and Thermal Histories

One of the variants of the cold dark matter (CDM) model of structure growth (designed to match the observed level of galaxy clustering on large scales together with the COBE results) is the cold+hot dark matter model (CHDM). For $\Omega_0 = 1$ ($\Omega_{hot}=0.3$, $\Omega_{cold}=0.6$, $\Omega_{baryon}=0.1$) Bryan et al. (1994) used a hydrodynamic plus N-body model to predict strong negative evolution of the 2-10 keV cluster XLF at $z=0.5$ and $L_X < 10^{44}$ erg s⁻¹. If we assume a similar level of evolution is predicted in the 0.5-2 keV band, then Bryan et al. predict $\alpha_D < -3$ in the parameterisation used here. Jing & Fang (1994) also predicted strong negative evolution of the cluster temperature function in the CHDM model. The observations presented here rule out these CHDM models, if taken at face value.

Furthermore, models in which the cluster gas simply scales as the mass distribution (e.g. Kaiser 1986) have difficulty in simultaneously reproducing the observed temperature function (Henry & Arnaud 1991) and XLF properties. This latter problem can be helped by assuming that the central gas entropy is largely due to heat input at an early epoch (e.g. Evrard 1990, Kaiser 1991) after which the gas settles adiabatically into the dark matter potential wells and is little heated by subsequent merger shocks. The X-ray gas distribution within the cluster is then more dependent on the total cluster potential than the density profile of the dark matter (which increases as $(1+z)^3$) and the cluster XLF is expected to show some negative evolution. Independently, recent observations of cluster gas metallicities (e.g. Loewenstein & Mushotzky 1996) have provided good evidence that the widely distributed metals were produced by type II supernovae with an energy budget sufficient to provide significant heating at some epoch $z \gtrsim 2$. Measurements of the cluster $L_X - T$ relationship at $z = 0.4$ (Mushotzky & Scharf 1997) for

luminous clusters ($L_{bol} \simeq 3 \times 10^{45} \text{ erg s}^{-1}$) show no evidence for evolution from $z = 0$, and no evolution of the temperature function has been found by Henry (1997) up to $z = 0.33$, in accord with a preheating scenario.

One result of the Kaiser (1991) preheating model is that much weaker negative evolution of the XLF is expected for clusters of luminosity below $10^{45} \text{ erg s}^{-1}$. This prediction is supported by Bower (1997) whose ‘constant entropy’ model for $n=-1$ and $\Omega_0=1$ actually predicts mild positive evolution of the differential XLF for $L_X \approx 10^{44} \text{ erg s}^{-1}$, but negative evolution by a factor ≈ 3 for $L_X \approx 4 \times 10^{44} - 10^{45} \text{ erg s}^{-1}$, as observed. This prediction is in good, qualitative, agreement with the results presented here which therefore provide the first confirming evidence for this type of thermal history, based on cluster population statistics alone.

Mathiesen & Evrard (1997) have used the WARPS $\log(N)$ - $\log(S)$ data of all clusters, as presented here, together with the updated data of Rosati et al. (1995), to constrain the parameters of a semi-analytical model based on a total mass to X-ray luminosity relation of the form:

$$L_X = L_{15} M^p (1+z)^s$$

Mathiesen & Evrard use the Press-Schechter (1974) formalism to describe the rate of growth of dark matter halos, which includes merging as larger halos grow faster than nearby smaller halos and ‘swallow’ them. The Press-Schechter mass function is converted to a luminosity function using the above relation, and the parameters L_{15} and p are determined by fitting to the local XLF of Ebeling et al. (1997a). The parameter s describes the evolution of the luminosity-mass relation in co-moving coordinates and includes the combined effects of cooling of the ICM via the expansion of the Universe, together with any heating of the ICM from galaxy winds or cooling via cooling flows. A value of s of ≈ 3 is indicative of constant entropy of the ICM in the cluster core with redshift (Evrard & Henry 1991, Bower 1997). Two models which give good fits to the $\log(N)$ - $\log(S)$ data are shown in Figure 3. Model (a) has $\Omega_0=1$, $n=-1$, $s=6$ and no cosmological constant. Model (b) has $\Omega_0=0.3$, $n=-1$, $s=2$ and again no cosmological constant. Both models, although containing the evolution inherent in the Press-Schechter formalism and the evolution of the above luminosity-mass relation, give similar $\log(N)$ - $\log(S)$ predictions as a simple model in which the XLF does not evolve. Some of the evolutionary terms evidently work in opposite directions, partly cancelling each other.

Mathiesen & Evrard find that Ω_0 and s are constrained by the $\log(N)$ - $\log(S)$ data such that $\Omega_0=1$ requires $s \geq 3$ and $\Omega_0 < 0.2$ requires $s < 2.5$, and that these conclusions are relatively insensitive to the value of n and the presence of a cosmological constant in a flat Universe. So for $\Omega_0=1$, preheating of the X-ray gas to provide the initial cluster core entropy (and possibly further heating via cluster merger shocks or galaxy winds) is probably required, as found above. Less theoretical modelling has been performed for low Ω_0 , and it is difficult to comment in detail on whether models including preheating of the X-ray gas are preferred. The results of Mathieson & Evrard (1997) suggest that cooling mechanisms may be dominant if $\Omega_0 < 0.2$.

6.2. Predictions for future surveys

Figure 6 reinforces the rareness of high redshift, high luminosity clusters. Because the $\log(N)$ - $\log(S)$ relation of these clusters is so flat, surveys which probe to faint fluxes over even a relatively large area of sky are not an efficient way of finding them. A serendipitous survey at faint fluxes $\sim 10^{-14}$ erg cm $^{-2}$ s $^{-1}$ (eg XMM pointed observations) would need to cover 200 deg 2 in order to detect ~ 30 high redshift ($z > 0.3$), high luminosity ($> 3 \times 10^{44}$ erg s $^{-1}$) clusters if the negative evolution observed at $z \approx 0.33$ ($\alpha_D = -2$) continues to higher redshifts. These clusters would represent only 0.15% of all the X-ray sources. However, such a survey would detect ~ 1000 high redshift, low luminosity clusters, assuming no evolution at low luminosities. A more efficient way of finding high redshift, high luminosity clusters would be a large area (e.g. 5000 deg 2) survey at a relatively bright flux limit (e.g. 2×10^{-13} erg cm $^{-2}$ s $^{-1}$) with sufficient spatial resolution (< 20 arcsec) to resolve high redshift clusters (e.g. an XMM slew survey, or the ROSAT & ABRIXSAS All Sky Surveys if the spatial resolutions are adequate). Such a survey would provide an order of magnitude increase in the number of X-ray selected high redshift, high luminosity clusters: ≈ 200 clusters at $z > 0.3$ and $L_X > 3 \times 10^{44}$ erg s $^{-1}$ (of which ≈ 35 would be at $z > 0.7$) again assuming negative evolution continues to higher redshifts. They would represent 4% of all the X-ray sources.

7. Conclusions

We have presented initial results from an X-ray selected, flux and surface brightness limited, complete survey of clusters of galaxies at relatively faint X-ray fluxes. The $\log(N)$ - $\log(S)$ relation of the clusters is consistent with previous measurements at both brighter and fainter fluxes. We have obtained redshifts for most, but not all, of the candidate clusters above our limit in total flux of 6×10^{-14} erg cm $^{-2}$ s $^{-1}$ 0.5-2 keV, including 10 at $z > 0.3$ and a further 2 with estimated redshifts of $z > 0.3$. Based on the properties of nearby clusters and our surface brightness limit, we estimate that few clusters are missing from our survey, particularly at high redshifts. The X-ray luminosities of the high redshift clusters lie in the range $4 \times 10^{43} h_{50}^{-2}$ erg s $^{-1}$ to $2 \times 10^{44} h_{50}^{-2}$ erg s $^{-1}$, the luminosities of poor clusters. The number of high redshift, low luminosity clusters is consistent with no evolution of the X-ray luminosity function between redshifts of $z \approx 0.4$ and $z = 0$. Mild positive evolution at the faintest luminosities cannot be ruled out. A limit of a factor of < 1.7 (at 90% confidence) is placed on the amplitude of any pure negative density evolution of clusters of these luminosities. An alternative parameterisation is the density evolution index α_D of the XLF which is constrained to be $-1.2 < \alpha_D < +1.8$ (at 90% confidence) for low luminosities. This can be contrasted with the value of $-3.5 < \alpha_D < -1.3$ (at 90% confidence) for EMSS clusters at similar redshifts but higher luminosities ($> 3 \times 10^{44} h_{50}^{-2}$ erg s $^{-1}$).

In a simple interpretation, this difference in the evolution of the cluster XLF at low luminosities and at high luminosities supports the hierarchical model of the growth of structure in the Universe. When compared with detailed modelling, as performed by Kaiser (1991), Evrard

& Henry (1991), Bower (1997) and Mathiesen & Evrard (1997), this evolutionary pattern is matched by models in which the X-ray gas is preheated at some early epoch, at least for $\Omega_0=1$.

We suspect that the higher number of high redshift clusters found in this survey compared to that of Castander et al. (1995) is due to the higher sensitivity to low surface brightness X-ray emission of the source detection algorithm used here. Finally, we have investigated differences in the flux measurement methods used here, in the EMSS, and by Nichol et al. (1997). We find that the EMSS fluxes may have been underestimated by 20-30%, but that the EMSS sample still shows evidence of negative evolution at high luminosities. The WARPS and EMSS Log(N)-Log(S) relations for all clusters, while not inconsistent, are in better agreement if the EMSS fluxes are increased by this amount.

This project has benefitted from the help of many people. We thank Mike Irwin for APM data, Geraint Lewis, Lance Miller and Mike Read for obtaining INT identifications, Greg Wirth for last minute help with masks at Lick, Rem Stone for help at the Lick 40 inch telescope, the KPNO TAC and the staff at Kitt Peak, and Richard Mushotzky for stimulating discussions. We thank Ben Mathiesen & August Evrard for sharing and discussing their model results, and the referee, Alastair Edge, for useful comments. This research has made use of data obtained through the High Energy Astrophysics Science Archive Research Center Online Service, provided by the NASA/Goddard Space Flight Center, and through the STScI Digitized Sky Survey archive. Part of this work was performed while CAS and LRJ were supported at NASA/GSFC by Regular and Senior NRC Research Associateships respectively, and ESP was supported at NASA/GSFC by a USRA Visiting Scientist Fellowship. LRJ acknowledges support from the UK PPARC. HE acknowledges financial support from SAO contract SV4-64008.

A. Systematic differences in flux measurement methods

In order to investigate any possible systematic difference in the methods used to measure the cluster fluxes here and in the EMSS, we have measured the fluxes of the 14 EMSS clusters where the X-ray emission is fully contained within 18 arcmin of the centre of a ROSAT PSPC field (this is the area we analyze with VTP). We also compare our flux values with those obtained by Nichol et al (1997) who analyzed the same ROSAT data but used a different method to measure the fluxes.

We use two methods to measure the EMSS cluster fluxes. The first method is our standard VTP analysis as applied to all the PSPC fields within WARPS, including exposure maps in each of the 0.5-0.9 keV and 0.9-2 keV bands. When analyzing the VTP results, we select a threshold for each EMSS cluster as we did for the WARPS sources, and apply our standard correction from detected to total count rate using the estimated core radius of each cluster. To convert from count rate to flux outside our Galaxy, we use the column density appropriate for each cluster from

Dickey & Lockman (1990), a metallicity of 0.3 and measured temperatures where available, or the cluster X-ray luminosity-temperature relation within an iterative procedure to estimate the temperature. The temperatures range from 2.8 keV (estimated) to 10.2 keV (measured). We also use these temperatures and column densities to convert each cluster flux from our 0.5-2 keV band to the 0.3-3.5 keV EMSS band.

The second method is simple aperture photometry on the 0.5-2 keV PSPC images of the five EMSS clusters which were targets of ROSAT observations, i.e. in which the cluster was located at the centre of the PSPC field. We use a large, metric aperture of 4 Mpc radius (except for the lowest redshift cluster where we use a radius of 3 Mpc) to ensure that almost all of the cluster flux is measured directly and corrections for missing flux (which always require a model profile to be assumed) remain at the less than 10% level. The background photon list, together with the exposure time for each photon (from the exposure map) and the sky area associated with each photon (from its Voronoi cell), are used to define the background level in a region outside the aperture but within an off-axis angle of 15 arcmin. The total count rate from both source and background photon lists within the aperture is then measured, and the scaled background level from the background region as well as the flux from all non-cluster sources subtracted. A small correction is made for the cluster flux lost under non-cluster sources.

The results are given in Table 1. The WARPS method measures fluxes a mean factor of 1.33 ± 0.15 times higher than the EMSS method, 1.21 ± 0.07 times higher than the Nichol et al. method, but only 1.10 ± 0.03 times higher than the aperture photometry method. In other words, the aperture photometry gives fluxes that are significantly higher than those determined in the EMSS (by a factor of 1.21) and also higher than those determined by Nichol et al. (by a factor of 1.1). Since, for a pure King profile, some flux will still be outside our 4 Mpc aperture (6% falls outside 4 Mpc for a core radius of 250 kpc, 8% for 350 kpc) the quoted aperture photometry gives results consistent with the WARPS method.

We checked the aperture photometry by repeating the above procedure on ten fields where the target was a point source (a star or AGN) of PSPC count rate comparable to the EMSS clusters (from $0.007 \text{ count s}^{-1}$ to $0.59 \text{ count s}^{-1}$) and the exposure times were similar (8 ks to 25 ks). The count rates measured within a 11 arcmin radius aperture, corresponding to our 4 Mpc aperture at $z \sim 0.35$, were a mean factor of 1.02 ± 0.05 times higher than the VTP ‘detected’ count rates, significantly lower than the mean increase in count rate found for the EMSS clusters (a factor of 1.11 ± 0.03). Also, the mean VTP ‘background’ count rates in the apertures (i.e. including the true background plus the cluster flux undetected by VTP) were a factor of $0.6 \pm 1.8\%$ lower than in the background regions in the point source fields, compared with $12 \pm 5\%$ higher in the 5 EMSS cluster fields. Thus mirror scattering in the wings of the PSF was not causing the increased count rates in the cluster fields. In addition, a comparison of 8 point-source fluxes measured by VTP and by Ciliegi et al. (1997) using the same PSPC data gave results consistent to within 3%. We also used the standard ROSAT data products (the 0.5-2 keV image and the ‘mex’ exposure map) to measure the flux within large apertures for two clusters, interactively subtracting non-cluster

sources and interpolating under them. For both MS0015.9+1609 & MS0735.6+7421 we found a count rate within 5 Mpc which agreed with the WARPS method to within 2%.

The systematic difference of 20%-30% between the WARPS flux measurements and the EMSS measurements explains the difference seen in the log(N)-log(S) relations. Simple aperture photometry seems to support the WARPS measurements.

There is a major difference in the WARPS method and that of Nichol et al. and the EMSS. Both Nichol et al. and the EMSS assumed a fixed core radius of 250 kpc for all clusters, whereas we estimate the core radius from the data. The method we use to estimate the core radius is over-simplified because it is designed for low signal-noise detections. Nevertheless, we find a wide range of core radii within this EMSS sub-sample, from 0 kpc to 245 kpc. For the two clusters mentioned in the introduction (MS2137.3-2353 & MS1512.4+3647), where HRI measurements show there are components with small core radii (17 ± 8 arcsec or 95 kpc and 7 ± 1.5 arcsec or 43 kpc) we find values of 30 kpc and 80 kpc. While these measurements may be inaccurate, or may reflect multiple components with different spatial distributions (eg cooling flows or point sources), they are in any case very different from 250 kpc. Thus the difference between the WARPS fluxes on the one hand and the EMSS and Nichol et al. fluxes on the other may result from the different treatments of the core radius.

B. X-ray K-corrections

Because not all of the WARPS clusters have measured redshifts, we adopt the approach of including the K-corrections in the models. K-corrections were calculated using for the 0.5-2 keV band using the optically thin thermal MEKAL model spectra of Kaastra (1992) and Mewe et al. (1986) with metal abundances set to 0.3 times cosmic abundance. The K-correction was defined here as

$$K_{0.5-2} = \frac{\int_{0.5}^2 f_{h\nu} d(h\nu)}{\int_{0.5(1+z)}^{2(1+z)} f_{h\nu} d(h\nu)}$$

where the integration limits are photon energies in keV. The results are shown in Figure 7. For redshifts up to $z=1$, the K-corrections are small ($<20\%$) for clusters of luminosity $\sim 10^{44} h_{50}^{-2}$ erg s $^{-1}$, and thus a temperature of ~ 3 keV. We include the K-corrections in the models by assigning a temperature to each luminosity based on the temperature-luminosity relation of White (1996): $T(\text{keV})=2.55 \times (L_{44} h_{50}^2)^{0.356}$ where L_{44} is the X-ray luminosity in units of 10^{44} erg s $^{-1}$. This relation is valid for luminosities of $\sim 10^{43} h_{50}^{-2}$ erg s $^{-1}$ to $\sim 10^{45} h_{50}^{-2}$ erg s $^{-1}$ and is in reasonable agreement with the L_X -T relation of Henry & Arnaud (1991).

The dashed line in Figure 7 shows the K-corrections obtained using a power law spectrum of energy index 0.5, as used by e.g. Henry et al. (1992). Although this is a good approximation

for the high temperature clusters more typical of the EMSS, it systematically underestimates the flux of clusters of temperature $T \sim 2$ keV (or $L \sim 5 \times 10^{43} h_{50}^{-2}$ erg s $^{-1}$) by $\approx 20\%$ at a redshift of $z=0.45$, the highest redshift at which the flux from such a cluster would be above the WARPS flux limit. The K-correction for clusters of even lower temperature (≤ 1 keV) becomes large (>1.5) at redshifts $z > 0.8$, because at this temperature most of the emission occurs at rest photon energies of < 2 keV, and is dominated by iron L shell line emission at ~ 1 keV at rest. In general, these large K-corrections are not needed here because at these very high redshifts, the low temperature, low luminosity systems fall below the survey flux limit. However, the detected soft X-ray emission of clusters containing cooling flows may be dominated by gas at or below a temperature of 1 keV. In general, the sensitivity of X-ray surveys (or at least those which use a lower energy bound > 0.5 keV) to high redshift cooling flows will be reduced by the K-correction of the cool component.

REFERENCES

- Bower, R. 1997, MNRAS, in press.
- Briel, U.G. et al. 1995, The ROSAT Users Handbook, MPE.
- Bryan, G.L., Klypin, A., Loken, C., Norman, M., Burns, J.O., 1994, ApJ, 437, 5L.
- Castander, F.J., Bower, R.G., Ellis, R.S., Aragon-Salamanca, A., Mason, K.O., Hasinger, G., McMahon, R.G., Carrera, F.J., Mittaz, J.P.D., Perez-Fournon, I., Lehto, H.J. 1995, Nature, 377, 39.
- Ciliegi, P., Elvis, M., Wilkes, B.J., Boyle, B.J. & McMahon, R.G., 1997, MNRAS, 284, 401.
- Collins, C.A., Burke, D.J., Romer, A.K., Sharples, R.M., Nichol, R.C. 1997, ApJ 479, L117.
- Couch, W.J., Ellis, R.S., Malin, D.F., & Maclaren, I. 1991, MNRAS 249, 606.
- Dickey J.M., Lockman F.J. 1990, ARA&A, 28, 215
- Ebeling, H., & Wiedenmann, G., 1993, Phys. Rev. 47, 704.
- Ebeling, H., Bohringer, H., Briel, U.G., Voges, W., Edge, A.C., Fabian, A.C., Allen, S.W. 1995, *Wide Field Spectroscopy and the Distant Universe*, S.J. Maddox & A. Aragon-Salamanca (eds), World Scientific, p. 221.
- Ebeling H., Voges, W., Böhringer H., Edge A.C., Huchra J.P., Briel U.G. 1996, MNRAS, 281, 799
- Ebeling, H., Edge, A.C., Fabian, A.C., Allen, S.W., Crawford, C.S. & Bohringer, H. 1997a, ApJ, 479, L101
- Ebeling, H., Edge, A.C., Bohringer, H., Allen, S.W., Crawford, C.S., Fabian, A.C., Voges, W. & Huchra, J.P. 1997b, MNRAS, submitted.
- Edge, A.C., Stewart, G.C., Fabian, A.C., Anruad, K.A., 1990, MNRAS, 245, 559.
- Edge, A.C., Stewart, G.C., Fabian, A.C., 1992, MNRAS, 258, 177.
- Efstathiou, G. and Rees, M. 1988, MNRAS, 230, 5p.
- Evrard, A.E. 1990, ApJ 363, 349.
- Evrard, A.E. & Henry, J.P., 1991, ApJ, 383, 95.
- Gioia, I., Henry, J.P., Maccacaro, T., Morris, S.L., Stocke, J.T., 1990, ApJ 357, L35.
- Gunn, J.E., Hoessel, J.G. & Oke, J.B. 1986, ApJ, 306, 30.
- Hamana, T., Hattori, M., Ebeling, H., Henry, J.P., Futamase, T., Shioya, Y., 1997, ApJ, 484, 574.
- Henry, J.P. & Arnaud, K.A. 1991, ApJ 372, 410.
- Henry, J.P., Gioia, I.M., Maccacaro, T., Morris, S.L., Stocke, J.T., Wolter, A. 1992, ApJ, 386, 408.
- Henry, J.P., 1997, ApJL, accepted.
- Hoessel, J.G., Gunn, J.E. & Thuan, T.X., 1980, ApJ 241, 486.

- Irwin M., Maddox S. & McMahon, R. 1994, Newsletter of the Royal Observatories, Spectrum no. 2, p.14
- Jing, Y-P. & Fang, L-Z 1994, ApJ 432, 438.
- Jones, C. & Forman, W., 1984 ApJ 276, 38.
- Jones, L.R., Fong, R., Shanks, T., Ellis, R.S., & Peterson, B.A. 1991, MNRAS 249, 481.
- Kaastra, J.S. 1992, An X-Ray Spectral Code for Optically Thin Plasmas (Internal SRON-Leiden Report, updated version 2.0)
- Kaiser, N., 1986, MNRAS, 222, 323.
- Kaiser, N., 1991, MNRAS, 383, 104.
- Kitayama, T. & Suto, Y. 1996, ApJ 469, 480.
- Kriss et al 1983, ApJ 272, 439.
- Loewenstein, M., Mushotzky, R.F., 1996, ApJ, 466, 695.
- Luppino, G.A. & Gioia, I.M. 1995, ApJ 445, L77.
- Mathiesen, B. Evrard, A. E. 1997, ApJ, in press.
- Mewe, R., Lemen, J.R., and van den Oord, G.H.J. 1986, A&AS, 65, 511.
- Mulchaey, J.S, Davis, D., Mushotzky, R.F. & Burstein, D. 1996, ApJ, 456, 80.
- Murdoch, H.S., Crawford, D.F., Jauncey, D.L. 1973, ApJ 183, 1.
- Mushotzky, R.F. & Scharf, C. 1997, ApJ, submitted.
- Nichol, R.C., Holden, B.P., Romer, A.K., Ulmer, M.P., Burke, D.J., Collins, C.A. 1997, ApJ 481, 644.
- Peacock, J. 1991. The Space Distribution of Quasars, ed, D. Crampton, ASP Conference Series Vol 21, p. 379.
- Piccinotti, G., Mushotzky, R.F., Boldt, E.A., Holt, S.S., Marshall, F.E., Serlemitsos, P.J. & Shafer, R.A., 1982, ApJ, 253, 485.
- Postman, M., Lubin, L.M., Gunn, J.E., Oke, J.B., Hoessel, J.G., Schneider, D.P. & Christensen, J.A. 1996, AJ, 111, 2.
- Press, W.H. & Schechter, P.L., 1974, ApJ 187, 425.
- Raymond, J.C. & Smith, B.W. 1977, ApJS, 35, 419.
- Rosati, P., Della Ceca, R., Burg, R., Norman, C., Giacconi, R., 1995, ApJ, 445, L11.
- Sandage, A., 1972, ApJ, 178, 1.
- Scharf, C., Jones, L.R., Ebeling, H., Perlman, E., Malkan, M. & Wegner, G. 1997, ApJ, 477, 79. (Paper I).
- Shanks, T., Georgantopoulos, I. Stewart, G. C., Pounds, K. A., Boyle, B. J., Griffiths, R. E., 1991, Nature, 353, 315.

White, D.A., 1996, Proceedings of Roentgenstrahlung from the Universe, eds Zimmerman, H., Trumper, J., Yorke, H., MPE report 263, 621.

Fig. 1.— The total, corrected (unabsorbed) flux of cluster candidates (assuming a King profile for extended sources and the instrumental PSF for point sources) versus their raw, detected, absorbed flux. The adopted flux limit of 3.5×10^{-14} erg cm $^{-2}$ s $^{-1}$ (0.5-2 keV) in detected flux results in a flux limit of 6×10^{-14} erg cm $^{-2}$ s $^{-1}$ (0.5-2 keV) in total flux.

Fig. 2.— Cluster integral Log(N)-Log(S) relation for various surveys including WARPS (heavy filled circles). The two solid curves are no evolution predictions for $q_0=0$ (upper) and $q_0=0.5$ (lower). The long dashed line is an extrapolation of the Log(N)-Log(S) relation at bright fluxes. The short dashed line just above the WARPS points indicates their maximum value if all the currently unidentified ‘possible’ candidates are clusters.

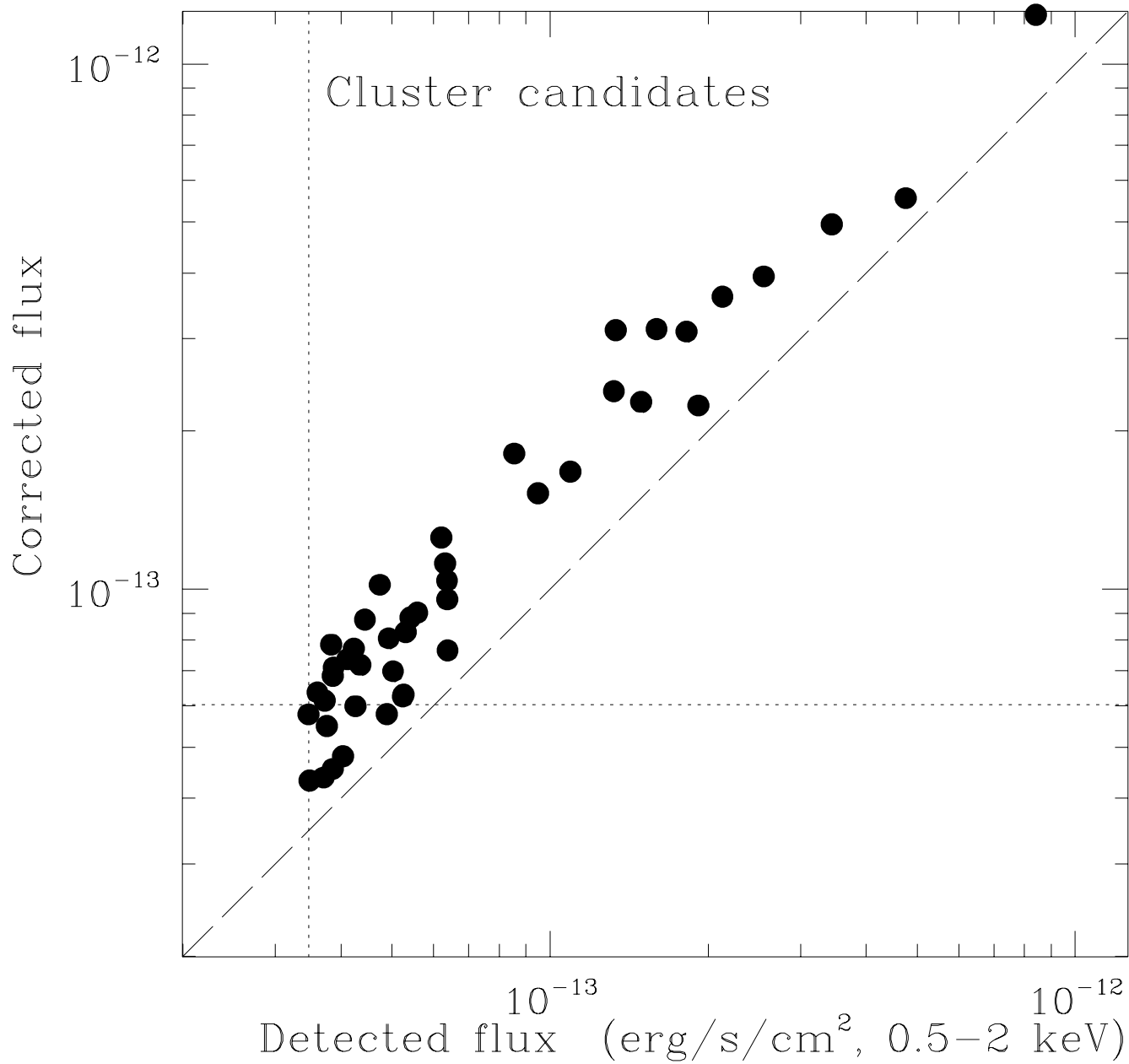
Fig. 3.— Cluster differential Log(N)-Log(S) relation showing the same data as in Figure 2. The solid curve is again a no evolution prediction for $q_0=0.5$. The Mathiesen & Evrard (1997) models are described in the text.

Fig. 4.— High redshift ($z>0.3$) cluster differential Log(N)-Log(S) relation. The solid curve is a no evolution prediction for $q_0=0.5$. The long dashed curves are predictions based on a simple density evolution of the XLF $\phi(z)=\phi(0)(1+z)^{\alpha_D}$. The short dashed lines show the possible range of the WARPS Log(N)-Log(S).

Fig. 5.— High redshift ($z>0.3$) cluster differential Log(N)-Log(S) relation for low luminosity ($L_X < 3 \times 10^{44}$ erg s $^{-1}$) clusters only. The solid curve is a no evolution prediction for $q_0=0.5$, consistent with the data. The long dashed curves are predictions based on a simple density evolution model as in Figure 4.

Fig. 6.— High redshift ($z>0.3$) cluster differential Log(N)-Log(S) relation for high luminosity ($L_X > 3 \times 10^{44}$ erg s $^{-1}$) clusters only. The solid curve is a no evolution prediction for $q_0=0.5$, which is inconsistent with the data. The long dashed curves are predictions based on a simple density evolution model as in Figure 4.

Fig. 7.— X-ray K-corrections for the 0.5-2 keV band as a function of cluster temperature as included in the model predictions. The K-correction definition and description is given in the Appendix.



Cluster	ROSAT ROR	z	WARPS		EMSS	Nichol et al.	Aperture ^a		WARPS	WARPS	WARPS
			0.5-2 keV	0.3-3.5 keV	0.3-3.5 keV	0.3-3.5 keV	0.5-2 keV	0.3-3.5 keV	EMSS	Nichol et al.	Aperture
MS0015.9+1609	rp800253n00	0.546	1.199	2.185	1.160	1.528	1.061	1.932	1.88	1.43	1.13
MS0451.5+0250	rp800480n00	0.202	5.680	10.514	3.992	5.730			2.63	1.83	
MS0451.6-0305	rp800229n00	0.550	1.163	2.153	1.557	1.544	1.082	2.003	1.38	1.39	1.08
MS0735.6+7421	rp800230n00	0.216	3.271	5.987	3.064	4.448	3.146	5.758	1.95	1.35	1.04
MS1020.7+6820	rp800641n00	0.201	0.574	0.974	0.682	0.791			1.43	1.23	
MS1201.5+2824	rp700232n00	0.167	0.956	1.631	1.694	1.747			0.96	0.93	
MS1208.7+3928	rp700277n00	0.340	0.293	0.507	0.411	0.427			1.23	1.19	
MS1219.9+7542	rp700434	0.240	0.143	0.231	0.519	0.317			0.44	0.73	
MS1308.8+3244	rp700216a00	0.245	0.507	0.872	0.693	0.749			1.26	1.16	
MS1335.2-2928	rp600188a02	0.189	0.321	0.525	0.843	0.539			0.62	0.97	
MS1358.4+6245	rp800109n00	0.328	1.219	2.186	2.327	1.792	1.027	1.842	0.94	1.22	1.19
MS1512.4+3647	rp700807n00	0.372	0.576	0.980	0.814	0.837			1.20	1.17	
MS2137.3-2353	rp800573n00	0.313	2.326	4.039	3.733	3.466	2.180	3.786	1.08	1.17	1.07
MS2255.7+2039	rp201282n00	0.288	0.519	0.907	0.576	0.739			1.58	1.23	
Mean									1.33±0.15	1.21±0.07	1.10±0.03

Table 1: Comparison of flux measurements of EMSS clusters.

NOTE.—All fluxes are in units of 10^{-12} erg cm $^{-2}$ s $^{-1}$.

^aA 4 Mpc radius aperture was used ($H_0=50$, $q_0=0.5$) except for MS0735.6+7421, for which a 3 Mpc radius was used.

Cluster $\text{Log}(N) - \text{Log}(S)$

